

QuOp_MPI: a framework for parallel simulation of quantum variational algorithms.

Edric Matwiejew^{a,*}, Jingbo B. Wang^a

^a*Department of Physics, The University of Western Australia, Perth, Australia*

Abstract

QuOp_MPI is a Python package designed for parallel simulation of quantum variational algorithms. It presents an object-orientated approach to quantum variational algorithm design and utilises MPI-parallelised sparse-matrix exponentiation, the fast Fourier transform and parallel gradient evaluation to achieve the highly efficient simulation of the fundamental unitary dynamics on massively parallel systems. In this article, we introduce QuOp_MPI and explore its application to the simulation of quantum algorithms designed to solve combinatorial optimisation algorithms including the Quantum Approximation Optimisation Algorithm, the Quantum Alternating Operator Ansatz, and the Quantum Walk-assisted Optimisation Algorithm.

Keywords: quantum algorithms, quantum walks, combinatorial optimization, parallel simulation, software packages

1. Introduction

With the first generation of quantum computers currently in operation, the start of a new computing paradigm appears just around the corner [1, 2]. Contributing to this optimism has been the development of algorithms that exploit a combination of classical and quantum hardware to solve optimisation problems [3–7]. As compared to many exclusively quantum algorithms, these Quantum Variational Algorithms (QVAs) require a minimal number of quantum operations and are inherently resilient to system noise [2, 8]. For these reasons, QVAs are strong contenders for early practical applications of quantum computing in the Noisy Intermediate Scale Quantum (NISQ) era [9]. Examples of such QVAs include the Quantum Approximate Optimisation Algorithm (QAOA) [3, 7], the Quantum Alternating Operator Ansatz (QAOAz) [4], and the Quantum Walk-assisted Optimisation Algorithm (QWOA) [5, 6], which have been designed to find optimal, or near-optimal, solutions to combinatorial optimisation problems.

Combinatorial Optimisation Problems (COPs) —the task of finding the best combination of items from a set—are nearly ubiquitous [10]. They are present in fields such as logistics [11], drug design [12], software compilation [13] and finance [14, 15]. These problems are difficult to solve classically due to a lack of identifiable structure and exponential growth of the solution space. QVAs are capable of providing a polynomial speedup as compared to a classical random search [5, 6]. This is an attractive prospect in the context of problems of great humanitarian or financial consequence.

To solve COPs, QVAs exploit quantum superposition to act on the complete problem-specific solution space in quantum parallel. They apply a sequence of alternating unitaries, which first encode the solution ‘qualities’ into the phase of superposed

quantum states, then ‘mix’ probability amplitude between these states. The phases-shift and mixing operations are parameterised by scalar variables that are adjusted iteratively by a classical optimiser that minimises with respect to the average measured solution quality. By encoding optimal solutions as minima in the solution space, a lowering of the average solution quality corresponds to amplification of probability density at quantum states associated with optimal or near-optimal solutions.

Classical numerical simulation plays a key role in the development of QVAs. Through simulation of the idealised quantum dynamics, researchers are able to study QVAs independently of implementation-specific hardware constraints and at scales that still exceed the functional limitations of current quantum hardware [16]. To assist with these efforts we have developed QuOp_MPI (**Q**uantum **O**ptimisation with **M**PI) [17], which provides a flexible framework for the design and classical simulation of QVAs.

There is currently significant interest in developing tools for the simulations of QVAs in a high-performance computing setting. Recent examples include TensorFlow Quantum a software framework for quantum machine learning [18] and the Jülich universal quantum computer simulator [16]. Both of these utilise GPU acceleration, with the latter being targeted at distributed GPU clusters. Also of note is the XACC framework and qFlex which utilise a tensor network approach to quantum simulation [19, 20]. These packages take a quantum-gate based approach to algorithm simulation and are capable of simulating QVAs with a large number of qubits (e.g. more than 50) given a quantum circuit structure that is parsimonious to their underlying simulation methods. QuOp_MPI presents a distinct option for QVA simulation in that it does not take a gate-based or approximative approach; instead, it focuses on the simulation of the fundamental unitary dynamics across the complete quantum state-space. It also provides the first tool for ready-made simulation of the Quantum Walk-assisted Optimisation Algorithm.

*Corresponding author.

E-mail address: Edric.Matwiejew@research.uwa.edu.au

The structure of the paper is as follows. In Section 2 we define the generalised QVA, introduce the QAOA, QAOAz and QWOA, and specify the problem of combinatorial optimisation. In Sections 3 and 4 we discuss the data structure algorithms and parallelisation schemes leveraged by QuOp_MPI. This is followed by an overview of the package structure, functionality and workflow types in Section 5. Section 6 we provide usage examples drawn from literature followed by a discussion of the package's performance in Section 7. Finally, concluding statements are presented in Section 8.

2. Theoretical Background

2.1. Quantum Variational Algorithms

For a quantum system of size $N = 2^n$, where integer n is a number of qubits with basis states $\left\{|0\rangle = \begin{pmatrix} 0 \\ 1 \end{pmatrix}, |1\rangle = \begin{pmatrix} 1 \\ 0 \end{pmatrix}\right\}$, QuOp_MPI defines a generalised QVA as

$$|\theta\rangle_{\text{ANZ}} = \left(\prod_{i=1}^D \hat{U}_{\text{ANZ}}(\theta_i) \right) |\psi_0\rangle_{\text{ANZ}}, \quad (1)$$

where $|\psi_0\rangle_{\text{ANZ}} \in \mathbb{C}^N$ is an initial quantum state with basis states $\{|i\rangle\}_{i=0,\dots,N-1}$, $\hat{U}_{\text{ANZ}} \in \mathbb{C}^{N \times N}$ is the ansatz¹ unitary, integer $D \geq 1$ specifies the number of applications of \hat{U}_{ANZ} to $|\psi_0\rangle_{\text{ANZ}}$ (the 'circuit depth') and $\theta = \{\theta_i \in \mathbb{R}\}$ is a set of classically optimised values that parameterise \hat{U}_{ANZ} . Together, \hat{U}_{ANZ} and $|\psi_0\rangle_{\text{ANZ}}$ define a specific QVA.

A QVA is executed by repeatedly preparing $|\theta\rangle_{\text{ANZ}}$ and measuring the expectation value

$$f_{\text{ANZ}}(\theta) = \langle \theta | \hat{Q} | \theta \rangle_{\text{ANZ}}, \quad (2)$$

where $\hat{Q} \in \mathbb{R}^{N \times N}$ is a diagonal operator whose entries $\text{diag}(\hat{Q}) = (q_i)$ specify the 'quality' associated with quantum state $|i\rangle$. The variational parameters θ are updated using a classical optimiser with the objective being minimisation of $f_{\text{ANZ}}(\theta)$.

The ansatz operator U_{ANZ} specifies a sequence of alternating unitaries. This can include phase-shifts

$$\hat{U}_{\text{phase}}(\gamma) = \exp(-i\gamma\hat{O}), \quad (3)$$

where $\hat{O} = \sum_{i=0}^{N-1} o_i |i\rangle\langle i|$ is a diagonal phase-shift operator, $\gamma \in \theta$ and \hat{U}_{phase} applies a phase-shift proportional to o_i . As well as mixing-unitaries

$$\hat{U}_{\text{mix}}(t) = \exp(-it\hat{W}), \quad (4)$$

where $t \in \theta$ is non-negative and $\hat{W} = \sum_{i,j=0}^{n-1} w_{ij} |j\rangle\langle i|$ is a mixing operator in which non-diagonal entries specify coupling between states $|i\rangle$ and $|j\rangle$. mixing-unitaries \hat{U}_{mix} drive the transfer of probability amplitude between quantum states, during which encoded phase differences contribute to constructive and destructive interference.

¹Originating from a German word that refers to the starting thought of a process. In mathematics, an ansatz is an educated guess or assumption made to help solve a problem.

Phase-shift operators \hat{O} and mixing operators \hat{W} may also be parameterised by θ . As these operators are time-independent Hamiltonians of the time-evolution operator, changes to the corresponding θ_i alter the element-wise magnitudes or structure of the matrix operator prior to computation of $|\theta\rangle$.

Typically, \hat{U}_{ANZ} is applied to $|\psi_0\rangle_{\text{ANZ}}$ D times with each repetition parameterised by a subset of the variational parameters $\theta \subseteq \theta$. Doing so increases the potential for constructive and destructive interference to concentrate probability amplitude at high-quality solutions; at the expense of classical optimisation over a larger parameter space and a deeper quantum circuit. In practice, a QVA must balance the increased convergence afforded by a higher D against the ability of the quantum hardware to maintain coherence over a longer sequence of quantum gates.

Sections 2.3 and 2.4 introduce four distinct QVAs with varying initial states, phase-shift unitaries and mixing-unitaries. We summarise here the following notational conventions for a given QVA 'ANZ':

- n : the number of qubits forming the 2^n dimensional Hilbert space \mathcal{H} of $|\psi_0\rangle_{\text{ANZ}}$.
- $|\psi_0\rangle_{\text{ANZ}}$: an initial quantum superposition in \mathcal{H} .
- \hat{U}_{ANZ} : a sequence of phase-shift and mixing operators of an arbitrary number, order and parameterisation values θ_i .
- θ : a set of $|\theta|$ variational parameters $\{\theta_i\}$ that parameterise \hat{U}_{ANZ} .
- $|\theta\rangle_{\text{ANZ}}$: the system state vector after $D \geq 1$ applications of U_{ANZ} .
- $f_{\text{ANZ}}(\theta_f) = \langle \theta_f | \hat{Q} | \theta_f \rangle_{\text{ANZ}}$: the value of the objective function with classically optimised variational parameters θ_f .

2.2. Combinatorial Optimisation with QVAs

Combinatorial optimisation problems seek optimal solutions \bar{s} of the form,

$$\bar{s} = \{s \mid C(s) \in \min \{C(s) \mid s \in \mathcal{S}'\}\}, \quad (5)$$

where the problem cost-function $C(s)$ maps a solution s from an ordered set of problem solutions $\mathcal{S} = \{s_i\}$ to \mathbb{R} , s is a k -permutation of discrete elements from a finite set ζ and

$$\mathcal{S}' = \{s \mid s \in \mathcal{X}\} \quad (6)$$

is the valid problem solution space where

$$\mathcal{X} = \bigcup_i \{s \mid \chi_i(s) = a_i\} \quad (7)$$

denotes any constraints on \bar{s} and $\mathbf{a} = \{a_i\}$ defines the constraints.

Problems of this type are often difficult to solve as \mathcal{S} grows factorially with $|\zeta|$ and, in general, lacks identifiable structure. For this reason, heuristic and metaheuristic algorithms are often used to find solutions that satisfy the relaxed condition of $C(\bar{s})$ being a 'sufficiently low' local minimum.

To apply a QVA to a given COP, an injective map is defined between \mathcal{S} and the Hilbert space of the quantum system \mathcal{H} with

the cost-function values forming the diagonal of the quality operator $\text{diag}(\hat{Q}) = C(s_i)$. For example, a problem with four solutions, $\mathcal{S} = \{s_0, s_1, s_2, s_3\}$, maps to a two-qubit system as

$$\begin{aligned} |00\rangle &= |0\rangle \rightarrow |s_0\rangle \\ |01\rangle &= |1\rangle \rightarrow |s_1\rangle \\ |10\rangle &= |2\rangle \rightarrow |s_2\rangle \\ |11\rangle &= |3\rangle \rightarrow |s_3\rangle, \end{aligned} \quad (8)$$

where $\text{diag}(\hat{Q}) = (C(s_0), C(s_1), C(s_2), C(s_3))$.

For a COP to be efficiently solvable by a QVA it must satisfy three conditions:

1. The number of solutions $|\mathcal{S}|$ must be efficiently computable in order to establish a bound on the size of the required Hilbert space \mathcal{H} .
2. For all solutions s , $C(s)$ must be polynomial-time computable.
3. For all solutions s , $C(s)$ must be polynomially bounded with respect to $|\mathcal{S}|$.

Conditions 1 and 2 ensure that the objective function (Equation (2)) is efficiently computable as classical computation of $C(s)$ is required to compute $f_{\text{ANZ}}(\theta)$ and boundedness in $C(s)$ ensures that the number of measurements required to accurately compute $f_{\text{ANZ}}(\theta)$ does not grow exponentially with $|\mathcal{S}'|$ [21]. These conditions constrain the application of QVAs to Polynomially Bounded (PB) COPs in the Non-deterministic Polynomial-time Optimisation problem (NPO) complexity class (together denoted as NPO-PB) [21].

2.3. Unconstrained Optimisation

We will first consider the case of unconstrained optimisation, where $\mathcal{S}' = \mathcal{S}$. For these COPs a quantum encoding of $C(s)$ is equivalent to a bijective map $\mathcal{S} \rightarrow \mathcal{H}$.

2.3.1. QAOA

The QAOA ansatz is comprised of two alternating unitaries. Firstly the phase-shift-unitary

$$\hat{U}_Q(\gamma_i) = \exp(-i\gamma_i \hat{Q}) \quad (9)$$

and, secondly, the mixing operator

$$\hat{U}_X(t_i) = \exp(-it_i \hat{W}_X), \quad (10)$$

where $\hat{W}_X = X^{\otimes N}$ and X is the Pauli- X (or NOT) gate. The mixing operator \hat{W}_{QAOA} induces a coupling topology that is equivalent to an n -dimension hypercube graph, as shown in Figure 1.

The initial state $|\psi_0\rangle_{\text{QAOA}}$ is prepared as an equal superposition over \mathcal{H} ,

$$|+\rangle = \frac{1}{\sqrt{n}} \sum_{i=0}^{n-1} |i\rangle. \quad (11)$$

The final quantum state is then

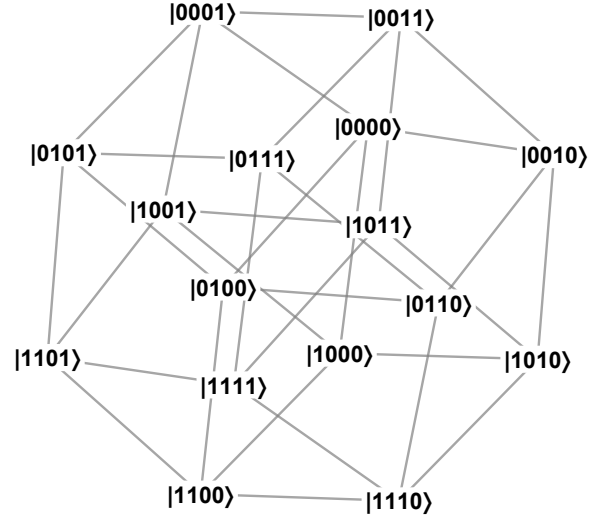


Figure 1: Coupling topology of W_X in the QAOA for $|\mathcal{S}| = 16$ (four qubits).

$$|\theta\rangle_{\text{QAOA}} = \left(\prod_{i=1}^D \hat{U}_X(t_i) \hat{U}_Q(\gamma_i) \right) |+\rangle, \quad (12)$$

where $\theta = \{\gamma_i, t_i\}$ and $|\theta| = 2D$ [3].

2.3.2. Extended-QAOA

A variation of the QAOA, ‘extended-QAOA’ (ex-QAOA) utilises a sequence of phase-shift unitaries,

$$\hat{U}_{\text{Qext}}(\gamma_i) = \prod_{j=1}^{|\Sigma|} \exp(-i(\gamma_i)_j \Sigma_j), \quad (13)$$

where Σ_j are non-identity terms in a Pauli-gate decomposition of \hat{Q} and $|\Sigma|$ is the number of non-identity terms [7]. This increases the number of variational parameters to $|\theta| = (1 + |\Sigma|)D$ with the intent of achieving a higher degree of convergence to optimal solutions at a lower circuit depth.

The final state of ex-QAOA ansatz is

$$|\theta\rangle_{\text{ex-QAOA}} = \left(\prod_{i=1}^D \hat{U}_X(t_i) \hat{U}_{\text{Qext}}(\gamma_i) \right) |+\rangle, \quad (14)$$

where $|+\rangle$ and \hat{U}_X are defined as in Equation (11) and Equation (10) and $\theta = \{\gamma_{ij}, t_i\}$.

2.4. Constrained Optimisation

We will now consider the case of constrained optimisation where, in general, $\mathcal{S}' \subset \mathcal{S}$. These algorithms implement χ by restricting the action of their mixing-unitaries and their initialisation of $|\psi_0\rangle_{\text{ANZ}}$ to a subspace of \mathcal{H} .

2.4.1. QAOA $_{\chi}$

The Quantum Alternating Operator Ansatz was developed to solve problems for which χ creates a correspondence between

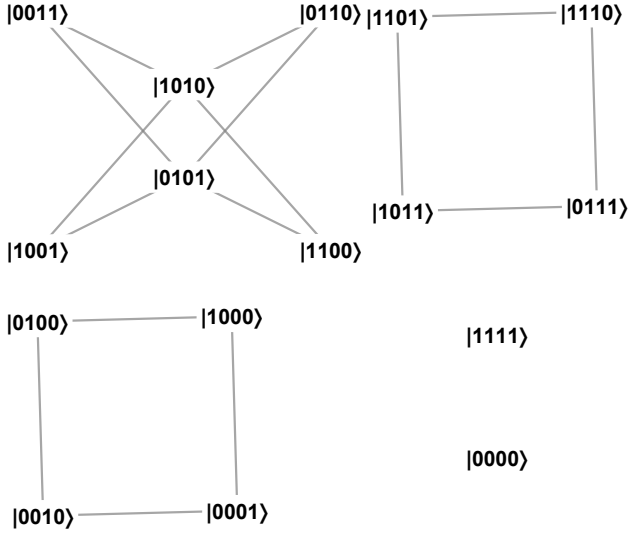


Figure 2: Coupling topology of the QAOAz mixing operators for a four-qubit system. Note that \mathcal{H} is partitioned into subgraphs of equal state parity.

S' and quantum states of equivalent parity – states with the same number of $|1\rangle$ states. This algorithm consists of the phase-shift-unitary defined in Equation (9), followed by a sequence of three mixing-unitaries with the mixing operators

$$\begin{aligned}\hat{B}_{\text{odd}} &= \sum_{a \text{ odd}}^{N-1} X_a X_{a+1} + Y_a Y_{a+1} \\ \hat{B}_{\text{even}} &= \sum_{a \text{ even}}^N X_a X_{a+1} + Y_a Y_{a+1} \\ \hat{B}_{\text{last}} &= \begin{cases} X_N X_1 + Y_N Y_1, & \text{odd} \\ I, & \text{Neven,} \end{cases}\end{aligned}\quad (15)$$

which together form the parity-conserving mixing operator

$$U_{\text{parity}}(t) = e^{-it\hat{B}_{\text{last}}} e^{-it\hat{B}_{\text{even}}} e^{-it\hat{B}_{\text{odd}}}\quad (16)$$

that mixes probability amplitude between subgraphs of equal parity as illustrated in Figure 2.

By initialising $|\psi_0\rangle_{\text{QAOAz}}$ in a quantum state that satisfies the parity constraint, probability amplitude is constrained to S' . The state evolution of the QAOAz is then

$$|\theta\rangle_{\text{QAOAz}} = \left(\prod_{i=1}^D \hat{U}_{\text{parity}}(t_i) \hat{U}_{\mathcal{Q}}(\gamma_i) \right) |\psi_0\rangle_{\text{QAOAz}}, \quad (17)$$

where $|\psi_0\rangle_{\text{QAOAz}}$ is an initial state satisfying the parity constraint [4].

2.4.2. QWOA

The Quantum Walk-assisted Optimisation Algorithm implements χ given the existence of an efficient indexing algorithm for all $s \in S'$. If so, the QWOA implements an indexing unitary

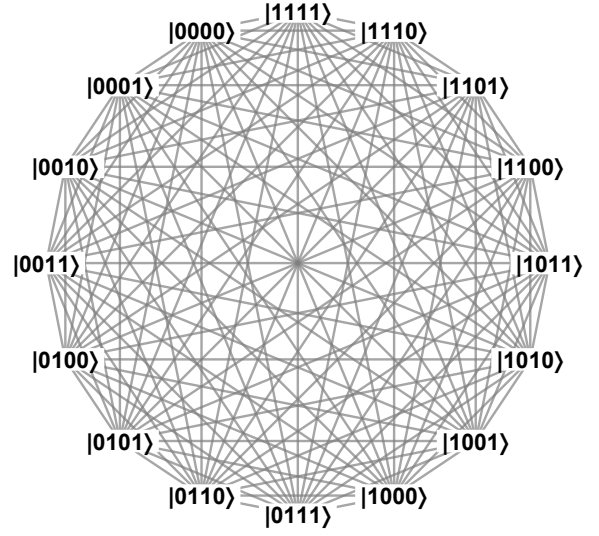


Figure 3: Coupling topology of the QWOA mixer for a system with $S' = 16$.

$$\hat{U}_{\#}^{\dagger}|i\rangle = \begin{cases} |\text{id}_{\chi}(i)\rangle, & |i\rangle \in |s'\rangle \\ |i\rangle, & \text{otherwise,} \end{cases}\quad (18)$$

where $\hat{U}_{\#}^{\dagger}$ maps states corresponding to valid solutions $|s'\rangle$ to indexed states $|\text{id}_{\chi}(i)\rangle$. By preparing $|\psi_0\rangle_{\text{QWOA}}$ as an equal superposition over $|\text{id}_{\chi}(i)\rangle$,

$$|\psi_0\rangle_{\text{QWOA}} = \frac{1}{\sqrt{|S'|}} \hat{U}_{\#}^{\dagger} \sum_{i=0}^{|S'|-1} |i\rangle, \quad (19)$$

probability amplitude is restricted to the subspace of indexed states.

The indexing unitary $U_{\#}^{\dagger}$ and its conjugate unindexing unitary $\hat{U}_{\#}$ occur either side of a mixing-unitary that acts on $|\text{id}_{\chi}(i)\rangle$:

$$\hat{U}_{\text{index}}(t) = \hat{U}_{\#} \exp(-it\hat{W}_{\text{QWOA}}) \hat{U}_{\#}^{\dagger}\quad (20)$$

Where efficiency in the implementation of $\hat{U}_{\#}$ dictates that \hat{W}_{QWOA} is circulant. Most commonly, \hat{W}_{QWOA} is chosen to be the adjacency matrix of the complete graph as it produces a maximal and unbiased coupling over $|S'\rangle$ (see Figure 3).

The state evolution of the QWOA is then

$$|\theta\rangle_{\text{QWOA}} = \prod_{i=1}^D \hat{U}_{\text{index}}(t_i) \hat{U}_{\mathcal{Q}}(\gamma_i) |\psi_0\rangle_{\text{QWOA}}, \quad (21)$$

where $\theta = \{\gamma_i, t_i\}$ and there are $|\theta| = 2D$ variational parameters [5, 6].

3. Numerical Methods

By default, QuOp_MPI presents three approaches by which to compute the action of a phase-shift or mixing-unitaries.

As the exponent matrix of phase-shift unitaries \hat{O} is diagonal, the action of a $\hat{U}_{\text{phase}}(\gamma_i)$ is efficiently computed in-Python via the Numpy package by noting that

$$\hat{U}_{\text{phase}}(\gamma)|\psi\rangle = \sum_i^{N-1} e^{-i\gamma o_i i} c_i |i\rangle, \quad (22)$$

where $|\psi\rangle$ is an arbitrary quantum state vector with complex coefficients c_i .

As a mixing-unitary must have non-diagonal entries in its matrix exponent \hat{W} , computation of $\hat{U}_{\text{mix}}(t_i)|\psi\rangle$ necessitates accurate computation of the action of the matrix exponential.

Given a circulant \hat{W} , QuOp_MPI takes advantage of the relationship between the eigensystem of circulant matrices and the discrete Fourier transform. The analytical solution for the eigenvalues of a circulant matrix are given by

$$\lambda_j = w_0 + w_{M-1}\omega^j + w_{M-2}\omega^{2j} + \dots + w_1\omega^{(M-1)j}, \quad (23)$$

where M is the size of the matrix, $w_{j=0,\dots,M-1}$ defines the first row of the circulant matrix, $\omega = \exp(\frac{2\pi i}{M})$ is a primitive M^{th} root of unity and $j = 0, \dots, M-1$. The corresponding eigenvectors,

$$v_j = \frac{1}{\sqrt{n}}(\omega^j, \omega^{2j}, \dots, \omega^{(n-1)j}), \quad (24)$$

then form the matrix of the discrete Fourier transform. As such, the action of a mixing-unitary with a circulant mixing operator may be implemented as

$$\hat{U}_{\text{mix}}(t)|\psi\rangle = F^{-1} e^{it\Lambda} F |\psi\rangle, \quad (25)$$

which is carried out in QuOp_MPI using algorithms provided by the Fastest Fourier Transform in the West (FFTW) library [22, 23].

For the case of sparse mixing operators, QuOp_MPI utilises a parallel implementation of a scaling and squaring algorithm, adapted from a parallel implementation previously developed by the authors [24].

The choice of initial values for θ , optimiser algorithm and optimiser algorithm hyper-parameters is an active area of research [25]. By default QuOp_MPI uses the Broyden-Fletcher-Goldfarb-Shanno algorithm [26] provided by SciPy via its ‘minimize’ function [27] as the authors have found it to behave reliably across a wide variety of QVAs (see Section 7). Users are able to adjust the parameters and optimisation algorithms used by the ‘minimize’ function or opt to use algorithms provided by the NLOpt package [28] through an included ‘SciPy-like’ interface [29].

4. Parallelisation Schemes

Parallelisation in QuOp_MPI is implemented using the Message Passing Interface (MPI) API. In general terms, MPI provides a distributed-memory model of parallel computing in which concurrent instances of the same program operate within isolated memory and spaces, communicating with each other

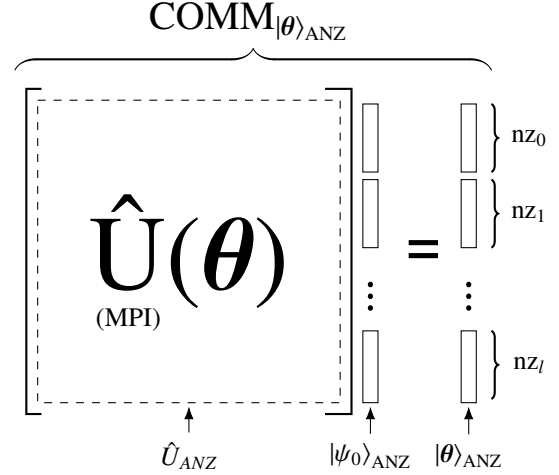


Figure 4: Diagrammatic representation of the partitioning of $|\psi_0\rangle_{\text{ANZ}}$ and $|\theta\rangle_{\text{ANZ}}$ over an MPI communicator of size l where nz_i denotes the number of vector elements stored at MPI rank i . Ansatz unitary, \hat{U}_{ANZ} , is implemented as an MPI function that acts on the distributed $|\psi_0\rangle_{\text{ANZ}}$ to return an identically partitioned $|\theta\rangle_{\text{ANZ}}$. Together, these components are denoted $\text{COMM}_{|\theta\rangle_{\text{ANZ}}}$.

using ‘message-passing’ directives. As opposed to shared-memory parallel frameworks, this allows for the use of large scale distributed computers (i.e. supercomputers).

Each program copy (or *MPI process*) is assigned a unique integer identifier (or *MPI rank* i_{COMM}) which, as a set, forms an *MPI communicator*. Within an MPI communicator, MPI node subsets (or *MPI sub-communicators*) may be created and assigned to parallel sub-tasks. The number of MPI processes in a given MPI communicator or MPI sub-communicator is referred to as the MPI communicator *size* nz . An MPI process is also commonly referred to as an *MPI node*; however, to maintain notational consistency, we will use *node* only to refer to *compute nodes* in a networked computational cluster. Depending on user-controlled settings, QuOp_MPI operates on the global MPI communicator or a variable configuration of MPI sub-communicators.

The primary parallelisation scheme $\text{COMM}_{|\theta\rangle_{\text{ANZ}}}$ is illustrated in Figure 4. The initial state $|\psi_0\rangle_{\text{ANZ}}$, evolved state $|\theta\rangle_{\text{ANZ}}$ and observable values $\text{diag}(\hat{Q})$ are evenly distributed over a communicator with each rank i_{COMM} containing nz sequential elements. The position of a local vector partition within the MPI communicator is thus specified by two variables; the number of vector elements in the local partition

$$\text{local_i} = nz_i \quad (26)$$

and their index offset

$$\text{local_i_offset} = \sum_{m=0}^{i_{\text{COMM}}-1} nz_m. \quad (27)$$

Unitary evolution is carried out using MPI-parallelised subroutines that act on the local vector partitions.

At run-time, QuOp_MPI attempts to partition the global vectors equally over each MPI rank in $\text{COMM}_{|\theta\rangle_{\text{ANZ}}}$ while satis-

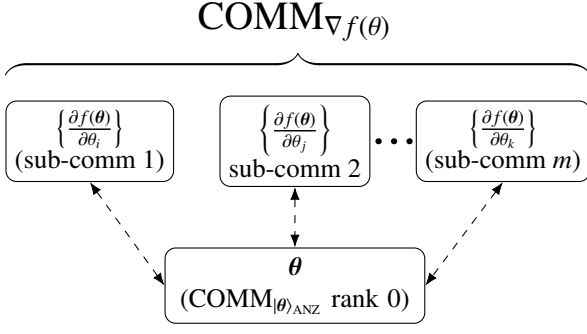


Figure 5: An example of the MPI communication topology used for parallel computation of $\nabla_{\theta} f_{\text{ANZ}}$. The objective function, $f_{\text{ANZ}}(\theta)$ is calculated by the $\text{COMM}_{|\theta|_{\text{ANZ}}}$ containing the root MPI process and its partial derivatives by sub-communicators 1 through to m where $m \leq \dim(\theta)$. Each sub-communicator implements an instance of $\text{COMM}_{|\theta|_{\text{ANZ}}}$.

fying any partitioning constraints associated with external libraries such as FFTW. If any of the nodes receive zero vector elements, they are excluded from $\text{COMM}_{|\theta|_{\text{ANZ}}}$ and the vector partitioning is recalculated. State evolution and calculation of the objective function $f_{\text{ANZ}}(\theta)$ is then carried out over $\text{COMM}_{|\theta|_{\text{ANZ}}}$ in parallel. With each evaluation of $|\theta\rangle_{\text{ANZ}}$, $f_{\text{ANZ}}(\theta)$ is sent to MPI rank 0 of $\text{COMM}_{|\theta|_{\text{ANZ}}}$ where it is received by the optimisation algorithm. The adjusted θ is then broadcast to all nodes in $\text{COMM}_{|\theta|_{\text{ANZ}}}$ and the cycle repeats until the optimisation algorithm terminates. The distributed $|\theta\rangle_{\text{ANZ}}$ may then be written to disk using parallel HDF5 or gathered at the root MPI rank.

In the case of optimisation algorithms that make use of gradient information, the user may choose to calculate the objective function gradient $\nabla_{\theta} f_{\text{ANZ}}$ in parallel. As shown in Figure 5, the global MPI communicator is split into P MPI sub-communicators of which $P - 1$ are assigned the task of approximating the partial derivative of $f_{\text{ANZ}}(\theta)$ (via forward or central differences) for a subset of θ . The MPI sub-communicator containing the root MPI process is responsible for the communication of the gradient evaluation points.

The number of created sub-communicators depends on the number of variational parameters $|\theta|$ and the number of compute nodes n_{node} in the global MPI communicator as follows:

1. If $|\theta| < N_{\text{node}} + 1$, assign each parameter in θ to a sub-communicator consisting of multiple nodes.
2. If $|\theta| > N_{\text{node}} + 1$, split ranks within nodes into sub-communicators, each assigned a parameter in θ .

This allows the user to specify a number of MPI processes that leads to an optimal sub-communicator size for their particular scale of QVA simulation.

5. Package Overview

QuOp_MPI is a Python module that provides an object-orientated approach to QVA design and parallel simulation. Foremost, it presents an approachable workflow in which users are able to write efficient and scalable quantum simulations

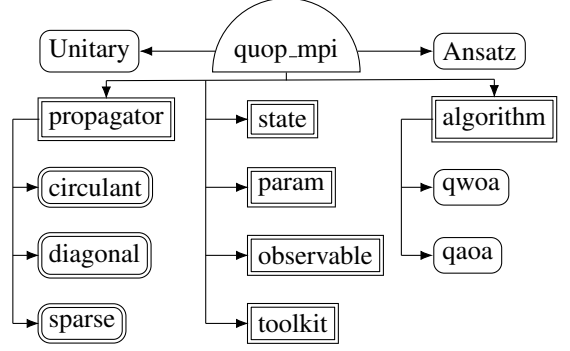


Figure 6: The user-level structure of the QuOp_MPI python package (imported as quop_mpi). Doubly outlined rectangles indicate submodules and singly outlined rectangles correspond to classes. Each `propagator` submodule contains a `Unitary` subclass and corresponding `operator` submodule.

without requiring prerequisite knowledge of compiled programming languages or parallel programming techniques. This is underpinned by generalised class structures and parallelisation schemes that have been designed to streamline the integration of additional parallel simulation methods.

The user-level structure of QuOp_MPI is shown in Figure 6. The package is centred around the `Ansatz` and `Unitary` classes. The `Ansatz` class manages the parallelisation scheme, definition, execution of the QVA and the recording of simulation results for a specific QVA. An overview of the `Ansatz` class is shown in Table 2.

The `Unitary` class provides a scaffolding with which parallel algorithms for the computation of the phase \hat{U}_{phase} and mixing \hat{U}_{mix} unitaries are integrated with QuOp_MPI. As shown in Table 3, a QuOp_MPI compatible `unitary` is implemented through the creation of a `Unitary` subclass which defines methods responsible for the calculation of the parallel partitioning scheme (see Section 4), computation of the action of the operator on the quantum state vector and management of the ancilla requirements of any external subroutines.

The `propagator` submodule contains predefined `Unitary` subclasses and an `operator` submodule contain functions for the generation of matrix operators \hat{O} or \hat{W} in a format that is compatible with the underlying numerical simulation methods of the corresponding `Unitary` subclass (see Section 3).

Submodules `state`, `param` and `observable` provide and functions that, when passed to the `Ansatz` class, define the initial quantum state $|\psi_0\rangle_{\text{ANZ}}$, initial variational parameters θ and quality operator \hat{Q} of a particular QVA.

Two predefined QVAs, `qwoa` and `qaoa`, are included in the `algorithm` submodule. These `Ansatz` subclasses implement the QWOA and QAOA respectively. The `toolkit` submodule provides convenience functions to assist in the calculation of matrix operators and quantum states involving the tensor product of Pauli matrices and bit-string qubit states.

Type: *operator*

Inputs: *args, **kwargs

Output: $(\hat{M}_{ij})_{\text{local.i.offset} < i < \text{local.i.offset} + \text{local.i}, j=0, N-1}$

Parallel generation of a mixing or phase-shift matrix operator \hat{M} . The positional argument *variational parameters* provides input for an arbitrary number of variational parameters. Input to the `Unitary` initialisation method. The matrix operator must be returned in a format that is compatible with the *propagate* method of a corresponding `Unitary` subclass.

Type: *observable*

Inputs: *args, **kwargs

Output: $(q_i)_{\text{local.i.offset} < i < \text{local.i.offset} + \text{local.i}}$

Parallel generation of $\text{diag}(\hat{Q})$. Input to the `Ansatz` *set_observables* method.

Type: *state*

Input: *args, **kwargs

Output: $(|\psi_0\rangle_i)_{\text{local.i.offset} < i < \text{local.i.offset} + \text{local.i}}$

Parallel generation of $|\psi_0\rangle_{\text{ANZ}}$, input to the `Ansatz` *set_initial_state* method.

Type: *param*

Input: int n_params, *args, **kwargs

Output: θ

Generation of θ for a particular \hat{U}_{MPI} , passed to the `Unitary` initialisation method. Required positional argument 'n_params' specifies the number of parameters $|\theta|$ associated with a given \hat{U}_{MPI} . Input to the `Unitary` initialisation method.

Table 1: QuOp.MPI function types. An arbitrary number of positional arguments (*args) are mapped to attributes of the either the `Unitary` and `Ansatz` class and keyword arguments (**kwargs) are defined by the user via the corresponding *set* or class initialisation method (see Table 2). Typical positional arguments of the *operator*, *observable*, *state* functions are 'system_size' (N), 'local_i' and 'local_i_offset'. Functions of type *observable*, *state* and *param* are required to return a NumPy array.

Finally, QuOp.MPI provides an additional layer of extensibility by supporting user-defined functions for the generation of \hat{O} , \hat{W} , \hat{Q} , θ and $|\psi_0\rangle_{\text{ANZ}}$, as shown in Table 1.

Within this structure, QuOp.MPI thus presents several levels of usage:

1. Simulation of the QWOA or QAOA using the `qwoa` or `qaoa` classes.
2. Simulation of the QWOA or QAOA using user-defined parallel functions.
3. Design and simulation of a QVA with the `Ansatz` class with or without user-defined parallel functions.
4. Integration of new state evolution methods for \hat{U}_{mix} or \hat{U}_{phase} through the creation of `Unitary` subclasses.

6. Usage Examples

The following examples are included with QuOp.MPI v1.0.0 [17]. As QuOp.MPI uses MPI, the example code should be executed using the 'mpiexec' or 'mpirun' command. For example, to run a Python program with an MPI communicator of size 2:

```
$: mpiexec -N 2 python3 program.py
```

6.1. The max-cut problem.

The max-cut problem seeks to partition the vertices of a graph such that a maximum number of neighbouring nodes are assigned to two disjoint sets. As our first example, we will demonstrate how QuOp.MPI can be used to simulate the prototypical application of the QAOA to this problem [3].

A quantum encoding of the max-cut problem is a bijective mapping of the vertices of a graph G to the qubits in \mathcal{H} with the set membership indicated by the corresponding qubit state. For example, a two vertex graph with vertices $\{0, 1\}$ has a solution space that is completely represented by an equal superposition over a two-qubit system: $\{\{0, 1\} \rightarrow |00\rangle, \{0\}, \{1\} \rightarrow |01\rangle, \{0\}, \{1\} \rightarrow |10\rangle \text{ and } \{0, 1\} \rightarrow |11\rangle$.

The cost function is then implemented as

$$C(s) = - \sum_{E(i,j) \in G} \frac{1}{2} (\mathbb{I} - Z_i Z_j), \quad (28)$$

where Z_i is a Pauli Z gate acting on the i^{th} qubit, $E(i, j)$ is an edge in G connecting vertex i to vertex j , and $Z_i Z_j$ has eigenvalue 1 if qubits i and j are in the same state or -1 otherwise.

6.1.1. QAOA

In Example (1) the QAOA is applied to the max-cut problem for the graph shown in Figure 7. The pre-defined `Ansatz` subclass `qaoa` forms the basis of the simulation.

To generate the graph and generate its adjacency matrix we use the external module 'networkx'. On lines 13 to 30, the cost function is defined. By using the 'I' and 'Z' functions from the `toolkit` submodule, we are able to explicitly compute the terms of Equation (28). Note that the adjacency graph 'G' and the matrices returned on lines 18 and 19 are in a SciPy sparse matrix format.

Lines 24 to 32 demonstrate standard use of the `qaoa` class. An instance of the class is instantiated for $N = \text{'system_size'}$. Next, the $\text{diag}(\hat{Q})$ is defined via the 'set_qualities' method. For this, we pass the 'serial' *observable* function along with a dictionary containing keyword arguments for the function. The 'serial' function assists with memory-efficient simulation given a serial cost-function by calling the function at the root MPI process and distributing its output over $\text{COMM}_{\theta_{\text{ANZ}}}$. The *ansatz* depth $D = 2$ is then defined via the 'set_depth' method.

Now that the `qaoa` instance is fully defined, simulation of the algorithm (as defined in Equation (12)) proceeds via the 'execute' method. By calling the 'execute' method without specifying θ we choose to use default *param* functions which generate random θ_i from a uniform distribution over $(0\pi, 2\pi]$.

set_unitaries [required]: Define the sequence of unitaries $\hat{U}_0\hat{U}_1...\hat{U}_M$.	gen_initial_params : Generate and return θ_0 .
set_observables [required]: Define measurement qualities $\text{diag}(\hat{Q})$.	evolve_state : Compute $ \theta\rangle_{\text{ANZ}}$.
set_initial_state [default $ \psi_0\rangle_{\text{ANZ}} = +\rangle$]: Define the initial quantum state $ \psi_0\rangle_{\text{ANZ}}$.	execute : Solve $\langle\theta_f \hat{Q} \theta_f\rangle_{\text{ANZ}} = \min(f_{\text{ANZ}}(\theta))$.
set_depth [default $D = 1$]: Define the number of ansatz repetitions D .	benchmark : Solve $\langle\theta_f \hat{Q} \theta_f\rangle_{\text{ANZ}}$ over $D = (d_{\min}, \dots, d_{\max})$.
set_optimiser [default SciPy BFGS, tol = 1^{-5}]: Specify the classical optimiser.	get_final_state : Return $ \theta_f\rangle_{\text{ANZ}}$ at $i_{\text{COMM}} = 0$ of $\text{COMM}_{ \theta\rangle_{\text{ANZ}}}$.
set_seed [default seed = 0]: Specify a random seed for QuOp_MPIfunctions.	get_probabilites : Return $\langle\theta_f\rangle$ at $i_{\text{COMM}} = 0$ of $\text{COMM}_{ \theta\rangle_{\text{ANZ}}}$.
set_parallel [default $\text{COMM}_{ \theta\rangle_{\text{ANZ}}}$ only]: Specify $\text{COMM}_{ \theta\rangle_{\text{ANZ}}}$ and/or $\text{COMM}_{\nabla f(\theta)}$.	get_expectation_value : Return $\langle\theta \hat{Q} \theta\rangle$ at $i_{\text{COMM}} = 0$ of $\text{COMM}_{ \theta\rangle_{\text{ANZ}}}$.
set_log [optional]: Specify a simulation output log.	save : Write $ \theta\rangle_{\text{ANZ}}$, $\text{diag}(\hat{Q})$, θ and the optimisation result to disk.
(un)set_observable_map [optional]: Define g in $\vec{q} = g(\text{diag}(\hat{Q}))$, where $g : \mathbb{R}^N \rightarrow \mathbb{R}^N$.	print_optimiser_result : Print the result summary of the classical optimiser.
(un)set_objective_map [optional]: Define h in $f_{\text{ANZ}}(\theta) = h(\langle\theta \hat{Q} \theta\rangle)$, where $h : \mathbb{R} \rightarrow \mathbb{R}$.	

Table 2: Public methods of the `Ansatz` class.

class unitary(Unitary):
self.plan(self, int N, MPI.COMM comm): Determine the parallel partitioning of $ \theta\rangle_{\text{ANZ}}$ and allocate memory required by external libraries (e.g. C, C++, or Fortran subroutines).
self.copy_plan(self, Unitary u): Copy the parallel partitioning scheme from an already initialised unitary.
self.propagate(self, float thetas): Compute $\hat{U}_{\text{MPI}} \psi\rangle$.
self.destroy(): Free allocated memory not managed by the Pythongarbage collector.

Table 3: User-defined methods required to define an `Unitary` subclass implementing a $\hat{U}_{\text{phase}}(\theta)$ or $\hat{U}_{\text{mix}}(\theta)$ unitary.

Finally, the optimiser result is displayed using the ‘print_optimiser_result’ method and the simulation results are saved to the HDF5 file ‘maxcut.h5’ under the ‘depth 2’ group.

The optimiser output is generated by the selected optimisation module which, by default, is SciPy’s ‘minimize’ configured to use the BFGS algorithm. The final value of the objective function (‘fun’) is approximately -19.25 (as compared to a starting expectation value of -12) with $\theta_f = (2.798, 3.312, 3.793, 1.214)$ (‘x’).

Figures 8 and 9, illustrates the initial and final probability distributions with respect to unique values of q_i . After application of the QAOA to the initial superposition, probability density is concentrated around the high-quality solutions with the optimal solution ($q = -24$) having the highest probability of measurement.

6.1.2. Extended-QAOA

Having demonstrated the effectiveness of the QAOA in finding high-quality max-cut solutions, we will now explore the application of the ex-QAOA to the same task. Example (2) demonstrates the implementation of ex-QAOA using the `Ansatz` class. As in Example (1), the graph and its adjacency matrix are generated using ‘networkx’.

The functions needed to implement Equation (13) and Equation (10) are defined from lines 18 to 26 and lines 28 to 29 respectively. The first of these, ‘maxcut_terms’, returns an array of the summation terms in Equation (28). The ‘maxcut_qualities’ function takes these terms as its input and returns $\text{diag}(\hat{Q})$.

QuOp_MPI/examples/maxcut/maxtcut.py

```

1 from quop_mpi.algorithm import qaoa
2 from quop_mpi import observable
3 from quop_mpi.toolkit import I, Z
4 import networkx as nx
5
6 Graph = nx.circular_ladder_graph(4)
7
8 vertices = len(Graph.nodes)
9 system_size = 2**vertices
10
11 G = nx.to_scipy_sparse_matrix(Graph)
12
13 def maxcut_qualities(G):
14     C = 0
15     for i in range(G.shape[0]):
16         for j in range(G.shape[0]):
17             if G[i,j] != 0:

```

```

18                 C += 0.5*(I(vertices) \
19                     - (Z(i,vertices) @ Z(j,vertices)))
20     return -C.diagonal()
21
22 alg = qaoa(system_size)
23
24 alg.set_qualities(
25     observable.serial,
26     {'function': maxcut_qualities,
27      'args': [G]})
28
29 alg.set_depth(2)
30 alg.execute()
31 alg.print_optimiser_result()
32 alg.save('maxcut', 'depth_2', 'w')

```

Example 1: Max-cut with the QAOA.

QuOp_MPI/examples/maxcut/plots.py

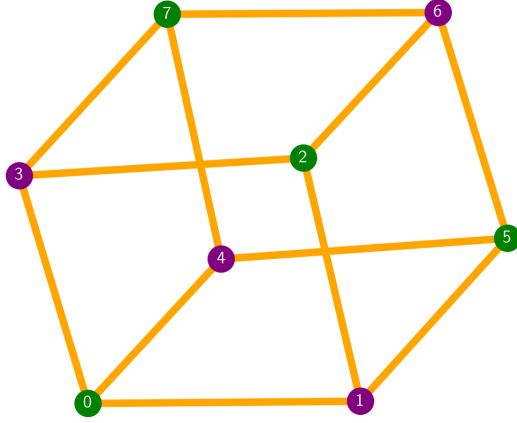


Figure 7: The graph generated for Example (1) and (2). The most probable optimised solution for the max-cut problem solved using the QAOA and ex-QAOA ($\vec{s} = (0, 1, 0, 1, 1, 0, 1, 0)$) is shown by vertex colouring with purple (darker) indicating a 0 and green (lighter) indicating a 1. The depicted vertex partitioning corresponds to the optimal solution for which $q_{90} = C(\vec{s}) = -24$.

A two-step calculation of the solution qualities is chosen as the ex-QAOA phase-shift operator associates a θ_i with each term of a Pauli-matrix decomposition of $\text{diag}(\hat{Q})$. The phase-shift-unitary is implemented using the `propagator` submodule `diagonal`. An instance of the `diagonal` unitary class ('UQ') is defined on lines 33 to 39. The first argument specifies the *operator* function responsible for generation of the Pauli-matrix terms Σ_j , the second specifies a dictionary of user-defined keyword arguments that are to be passed to the *operator* function, the third argument specifies the number of θ_i associated with 'UQ' and, finally, the fourth argument specifies the *param* function used for initialisation of the unitary's variational parameters. The *param* function generates θ as described in Section 6.1.1.

The *operator* function 'diagonal.serial' executes the serial 'maxcut_terms' function at the root MPI process and distributes the array of Pauli-matrix terms over $\text{COMM}_{|\theta|_{\text{ANZ}}}$. The

'unitary_n_params' keyword argument describes the number of operator terms returned by 'diagonal.serial', which are mapped to a sequence of \hat{U}_{phase} unitaries each parameterised by a unique θ_i .

Definition of the mixing-unitary 'UW' occurs on lines 41 to 43. As with 'UQ', the first argument specifies the *operator* function and the 'parameter_function' argument specifies the *param* function. The *operator* function 'sparse.operator.hypercube' generates a parallel-partitioned instance of the hypercube mixing operator (see Equation (20)).

On line 47 the defined unitaries 'UQ' and 'UW' are then passed to an instance of the `Ansatz` class via the 'set_unitaries' method ordered from left to right. The objection function is then defined by passing the 'maxcut_qualities' function to the 'set_observables' method.

The ex-QAOA simulation is then executed on line 54. Note that, as D has not been specified via the 'set_depth' method, the algorithm is run with the default ansatz depth of $D = 1$.

QuOp_MPI/examples/maxcut_extended/maxcut_extended_plots.py

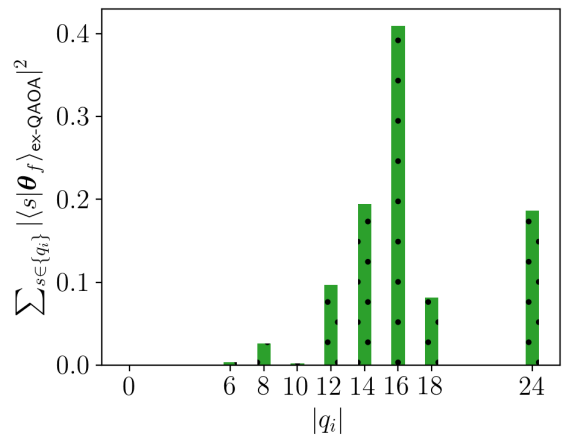


Figure 10: Final probability distribution of the max-cut solutions following execution of the ex-QAOA defined in Exercise (2).

```

1  from quop_mpi import Ansatz
2  from quop_mpi.propagator import diagonal, sparse
3  from quop_mpi.observable import serial
4  from quop_mpi.param.rand import uniform
5  from quop_mpi.toolkit import Z
6  import numpy as np
7  import networkx as nx
8
9  Graph = nx.circular_ladder_graph(4)
10 vertices = len(Graph.nodes)
11 system_size = 2*vertices
12
13 G = nx.to_scipy_sparse_matrix(Graph)
14
15 n_edges = 2*Graph.number_of_edges()
16
17 def maxcut_terms(G):
18     vertices = G.shape[0]
19     terms = []
20     for i in range(G.shape[0]):
21         for j in range(G.shape[0]):
22             if G[i,j] != 0:
23                 term = Z(i, vertices) @ Z(j, vertices)
24                 terms.append(-0.5*(1 - term.diagonal()))
25     return terms
26
27 def maxcut_qualities(terms):
28     return np.sum(terms, axis = 0)
29
30 computed_terms = maxcut_terms(G)
31
32 UQ = diagonal.unitary(
33     diagonal.operator.serial,
34     operator_kwargs = {
35         'function': maxcut_terms,
36         'args': [G]},
37     unitary_n_params = n_edges,
38     parameter_function = uniform)
39
40 UW = sparse.unitary(
41     sparse.operator.hypercube,
42     parameter_function = uniform)
43
44 alg = Ansatz(system_size)
45
46 alg.set_unitaries([UQ, UW])
47
48 alg.set_observables(
49     serial,
50     {'function': maxcut_qualities,
51      'args': [computed_terms]})
52
53 alg.execute()
54 alg.print_optimiser_result()
55 alg.save('maxcut_extended', 'depth_2', 'w')

```

Example 2: Max-cut with ex-QAOA.

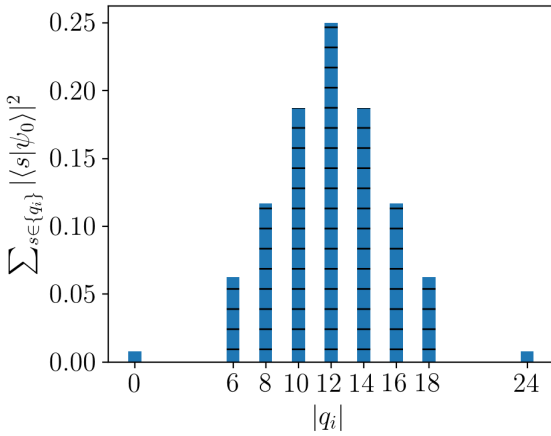


Figure 8: The initial solution probability distribution for the max-cut problem simulated in Examples (1) and (2).

6.1.3. Parallel computation of $C(s)$.

We conclude consideration of the max-cut problem by demonstrating how a user might modify their code in order to more efficiently generate the max-cut quality values. As a corollary of point 2 in Section 2.2 it will generally be the case that the calculation of any $C(s)$ may be performed independently from the rest of the cost function values. In such instances, the generation of $\text{diag}(\hat{Q})$ is an embarrassingly parallel problem and, as such, users are encouraged to implement their own parallel quality functions.

A parallel *observable* function for the max-cut problem is

shown in Example (3). It follows the structure described in Table 1, with the positional arguments being the `Ansatz` class attributes ‘system_size’, ‘local_i’ and ‘local_i_offset’, and the keyword arguments used to implement user-definable parameters. At run-time, this function is called by each rank in $\text{COMM}_{|\theta\rangle_{\text{ANZ}}}$ with the parameters ‘local_i’ and ‘local_i_offset’ used to generate q_i specific to that local partition.

To use ‘parallel_max-cut’ as part of a QAOA simulation the function is passed to the ‘set_qualities’ method as follows:

```

alg.set_qualities(
    parallel_maxcut_qualities,
    {'graph': G})

```

6.2. Portfolio Re-balancing

To explore the case of constrained optimisation using the QWOA and the QAOAz we will consider the problem of portfolio re-balancing. For each asset in a portfolio of size M , an investor must choose one of the following positions:

1. Short position: buying and selling an asset with the expectation that it will drop in value.
2. Long position: buying and holding the asset with the expectation that it will rise in value.
3. No position: taking neither the long or short position.

A quantum encoding of the possible solutions uses two qubits per asset.

1. $|01\rangle \rightarrow$ short position
2. $|10\rangle \rightarrow$ long position
3. $|00\rangle$ or $|11\rangle \rightarrow$ no position

QuOp_MPI/examples/maxcut/maxcut_parallel_qualities.py

```

1 def parallel_maxcut_qualities(
2     system_size, local_i,
3     local_i_offset, graph = G):
4
5     n_qubits = G.shape[0]
6     qualities = np.zeros(
7         local_i, dtype = np.float64)
8
9     start = local_i_offset
10    finish = local_i_offset + local_i
11
12    for i in range(start, finish):
13        bit_string = np.binary_repr(
14            i, width = n_qubits)
15        for j, bj in enumerate(bit_string):
16            for k, bk in enumerate(bit_string):
17                if G[j, k] != 0 and bj != bk:
18                    qualities[i] -= 1
19
20    return qualities

```

Example 3: User-defined quality function for the max-cut problem.

QuOp_MPI/examples/maxcut_plots.py

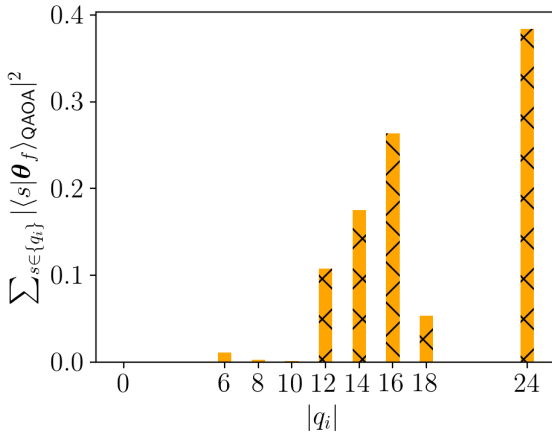


Figure 9: Solution quality probability distribution following the execution of the QAOA as simulated in Example (1).

The discrete mean-variance Markowitz model provides a means of evaluating the quality associated with a given combination of positions. It can be expressed through minimisation of the cost function,

$$C(s) = \omega \sum_{i,j=1}^M \sigma_{ij} Z_i Z_j - (1 - \omega) \sum_{i=1}^M r_i Z_i, \quad (29)$$

subject to the constraint,

$$\chi_{\text{asset}}(s) = \sum_{i=1}^M z_i. \quad (30)$$

In this formulation, the Pauli-Z gates Z_i encode a particular portfolio where, for each asset, eigenvalue $z_i \in \{1, -1, 0\}$ represents a choice of long, short or no position. Associated with each asset is the expected return r_i and covariance σ_{ij} between assets i and j ; which are calculated using historical data. The risk parameter, ω , weights consideration of r_i and σ_{ij} such that as $\omega \rightarrow 0$ the optimal portfolio is one providing maximum returns, while as $\omega \rightarrow 1$ the optimal portfolio is the one that minimises risk. The constraint $\chi_{\text{asset}}(s)$ works to maintain the relative net position with respect to a pre-existing portfolio [30].

In the following examples, we demonstrate the application of the QWOA and QAOAz to a small ‘portfolio’ consisting of four assets taken from the ASX 100, under the constraint $\chi_{\text{asset}}(s) = 2$.

6.2.1. Comparison of the QWOA and QAOAz.

As outlined in Section 2.4.2, QWOA uses an indexing unitary to encode constraints on the solution space. As QuOp_MPI is interested only in the abstracted unitary dynamics of the quantum state evolution, implementation of the indexing unitary simply requires that the user supply a quality function that returns the restricted solution space in a consistent order. For the QWOA example, the set of valid solutions was calculated using the program ‘qwoa_qualities.py’, which was originally written for [30]. It makes use of the pandas-webreader package [31] to source the daily adjusted close price of a given list of stocks from the Yahoo Finance website [32]. When run as the main program, ‘qwoa_qualities.py’ computes and returns the valid quality values (S') using historical data between user-specified dates and outputs $\text{diag}(\hat{Q})$ to a CSV file. For this example, the stocks AMP.AX, ANZ.AX and AMC.AX were considered between 1/1/2017 and 12/31/2018.

The QWOA algorithm is included with QuOp_MPI as a predefined module. As such, its simulation, shown in Example (4), is similar in structure to the QAOA program outlined in Section 6.1.1. However, as in this instance, because $\text{diag}(\hat{Q})$ is stored in a CSV file, we use the external package Pandas to read the quality values and the `diagonal_operator` function ‘serial_array’ to pass these values to the ‘set_qualities’ method on lines 12 to 14.

Note that the size of the simulation is determined by the number of valid solutions $|S'|$. This is distinct from a quantum implementation of the QWOA algorithm as, while its walk operation occurs over S' , its phase-shift operation still acts on S . However, because $|\psi_0\rangle_{\text{QWOA}}$ is initialised as an equal superposition over S' , quantum states associated with invalid solutions do not influence the idealised quantum dynamics. Hence, we can gain a significant performance advantage at no cost to simulation accuracy by restricting the classical simulation to S' .

In Section 6.1.1, $|\theta\rangle$ and \vec{q} were saved to a HDF5 file and analysis of algorithm performance was determined via computation on these arrays. Study of the complete quantum state is essential to understanding the dynamics associated with a particular QVA application, but often a researcher is concerned more immediately with $\langle \theta_f | \hat{Q} | \theta_f \rangle_{\text{ANZ}}$ with respect to changes in D or $|S'|$. For this reason QuOp_MPI supports the recording of important simulation metrics in a log file. Specified via the ‘set_log’ method on lines 16 to 19, the first argument specifies the name of the CSV output log file, the second argument specifies the simulation label and the third argument specifies the write action which follows the convention of ‘a’ to append or ‘w’ to (over)write. With a log file set the system size ($|\text{diag}(\hat{Q})|$), ansatz depth (D), final objective function value ($\langle \theta_f | \hat{Q} | \theta_f \rangle_{\text{ANZ}}$), state norm ($\langle \theta | \theta \rangle$), in-program simulation time, MPI communicator size, number of function evaluations and the success status of the optimiser are recorded for each simulation instance.

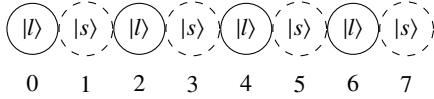
```

1 from quop_mpi.algorithm import qwoa
2 from quop_mpi import observable
3 import pandas as pd
4
5 qualities_df = pd.read_csv('qwoa-qualities.csv')
6 qualities = qualities_df.values[:,1]
7
8 system_size = len(qualities)
9
10 alg = qwoa(system_size)
11
12 alg.set_qualities(
13     observable.array,
14     {'array': qualities})
15
16 alg.set_log(
17     'qwoa_portfolio_log',
18     'qwoa',
19     action = 'w')
20
21 alg.benchmark(
22     range(1,6),
23     3,
24     param_persist = True,
25     filename = 'qwoa_portfolio',
26     save_action = 'w')
    
```

Example 4: Portfolio optimisation with the QWOA.

To study how $\langle \theta_f | \hat{Q} | \theta_f \rangle_{\text{QWOA}}$ changes as D increases we call the ‘benchmark’ method on lines 21 to 26. The first argument is an iterable object that provides a sequence of D values, the second is the number of repeat simulations at each D . The keyword arguments ‘filename’ and ‘save_action’ specify that $|\theta_f\rangle_{\text{QWOA}}$ and $\text{diag}(\hat{Q})$ be saved to the new HDF5 file ‘qwoa_portfolio.h5’. The ‘param_persist’ argument specifies a schema for the selections of the initial θ . If ‘True’ for all $D > 1$ the best-performing θ are used as the starting parameters for $D + 1$. If ‘False’ the θ are generated as per the default or user-specified param functions.

A QAOAz approach to the portfolio optimisation problem uses two parity mixers that act on the short and long qubits respectively such that the \mathcal{S} is partitioned into subgraphs of the same $\chi_{\text{asset}}(s)$ value. For this example, we are considering four assets so the two parity mixers act on separate subspaces of \mathcal{H} as shown below:



Where $|l\rangle$ denotes a ‘long’ qubit, $|s\rangle$ denotes a ‘short’ qubit and the numbering indicates the global index of each qubit.

To constrain probability amplitude to \mathcal{S} , $|\psi_0\rangle_{\text{QAOAz}}$ is prepared as

$$|\psi_0\rangle_{\text{QAOAz}} = |01\rangle^{\otimes A} \left(\frac{1}{\sqrt{2}} (|00\rangle + |11\rangle)^{2N-A} \right), \quad (31)$$

where A is the desired value of $\chi_{\text{asset}}(s)$. This creates a (non-equal) superposition of states across all qubit subgraphs with a net parity of A .

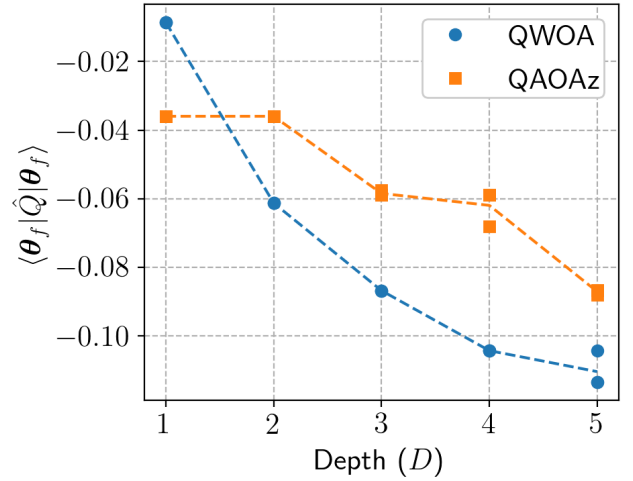
To implement this algorithm in QuOp_MPI we use the `Ansatz` class along with the `sparse` and `diagonal` `propagator` modules, the `observable` `state` and `param` submodules. The `toolkit` functions ‘string’, ‘X’ and ‘Y’ are used to define the parity mixers and initial state.

As with Example (4), the quality function is located in the external module ‘qaoaz_portfolio.py’ which is included in QuOp_MPI/examples/portfolio. It follows the same method as ‘qwoz_portfolio.py’, differing in that it has been written as a parallel quality function (see Section 6.1.3) that returns local partitions of the complete solution space \mathcal{S} .

The dual parity mixing operators are defined via three Python functions. The first of these (lines 13 to 11) defines a generalisation of the Pauli-matrix terms used for the B_{odd} , B_{even} and B_{last} mixing operations in Equation (10). The second function (lines 13 to 29) takes a

list of qubit indexes specifying a subspace of \mathcal{H} and the total number of qubits as its arguments and returns B_{odd} , B_{even} and B_{last} acting on the subspace. The third function, ‘portfolio_mixer’ (lines 43 to 48), takes a number of qubits as its argument. It partitions the input number of qubits into subgroups, as depicted in Figure 2, and returns a Python list containing the six mixing operators in the SciPy sparse CSR format.

A function to generate $|\psi_0\rangle_{\text{portfolio}}$ is defined on lines 50 to 57 where, on lines 52 and 53, the ‘kron_power’ function takes a NumPy array a and an integer N as its arguments and returns $a^{\otimes N}$ and, on line 54, the ‘string’ function generates a qubit state from its bit-string representation. The function ‘kron’, on line 56, takes a list of arrays and returns their tensor product.


 Figure 11: Optimised objective function value $\langle \theta_f | \hat{Q} | \theta_f \rangle$ for the portfolio rebalancing problem using QWOA and QAOz.

We then proceed to the definition of \hat{U}_{QAOAz} using the `Ansatz` class. An initial state other than an equal superposition is specified using the ‘set_initial_state’ method on line 77. It follows the same input convention as the previously described ‘set’ methods. The wrapper function ‘state.serial’ is used here to parse and distribute the output of the serial ‘parity_state’ function.

As, in this instance, the phase-shift unitaries’ matrix operator

```

1 from quop_mpi import Ansatz, observable, state, param
2 from quop_mpi.propagator import diagonal, sparse
3 from quop_mpi.toolkit import kron, kron_power
4 from quop_mpi.toolkit import string, X, Y
5 from qaoaz_qualities import qaoaz_portfolio
6 from numpy import sqrt
7
8 def parity_ring(i, j, n_qubits):
9     parity = X(i, n_qubits) @ X(j, n_qubits) \
10         + Y(i, n_qubits) @ Y(j, n_qubits)
11     return parity
12
13 def parity_mixer(qubits, n_qubits):
14
15     odd = 0
16     even = 0
17
18     n_subset = len(qubits)
19
20     for i in range(n_subset - 1):
21
22         if (i % 2 != 0):
23             odd += parity_ring(qubits[i],
24                               qubits[(i + 1) % n_subset],
25                               n_qubits)
26
27         elif i % 2 == 0:
28             even += parity_ring(qubits[i],
29                                qubits[(i + 1) % n_subset],
30                                n_qubits)
31
32     mixer = [odd, even]
33
34     if len(qubits) % 2 != 0:
35         last = parity_ring(qubits[-1],
36                            qubits[1],
37                            n_qubits)
38
39     mixer.append(last)
40
41     return mixer
42
43 def mixer(n_qubits):
44     short_qubits = [i for i in range(0, n_qubits, 2)]
45     long_qubits = [i for i in range(1, n_qubits, 2)]
46     short_mixer = parity_mixer(short_qubits, n_qubits)
47     long_mixer = parity_mixer(long_qubits, n_qubits)
48     return short_mixer + long_mixer
49
50 def parity_state(n_qubits, D):
51     M = n_qubits // 2
52     term_1 = kron_power(string('01'), D)
53     term_2 = kron_power(
54         1/sqrt(2) * (string('11') + string('00')),
55         M-D)
56     state = kron([term_1, term_2])
57     return state
58
59 n_qubits = 8
60 system_size = 2*n_qubits
61
62 UQ = diagonal.unitary(
63     qaoaz_portfolio,
64     parameter_function = param.rand.uniform)
65
66 UW = sparse.unitary(
67     sparse.operator.serial,
68     operator_kwargs = {
69         'function': mixer,
70         'args': [n_qubits]},
71     parameter_function = param.rand.uniform)
72
73 alg = Ansatz(system_size)
74
75 alg.set_unitaries([UQ, UW])
76
77 alg.set_initial_state(
78     state.serial,
79     {'function': parity_state,
80      'args': [n_qubits, 2]})
81
82 alg.set_observables(0)
83
84 alg.set_log(
85     'qaoaz_portfolio_log',
86     'qaoaz',
87     action = 'w')
88
89 alg.benchmark(
90     range(1, 6),
91     3,
92     param_persist = True,
93     filename = 'qaoaz_portfolio',
94     save_action = 'w')

```

Example 5: Portfolio optimisation with the QAOAz.

is equal to $\text{diag}(\hat{Q})$, the objective function is defined by calling ‘set_observables’ on line 82 with an integer argument that specifies the position of the mixing operator in the input list of unitaries (line 75).

Finally, an output log is specified and the benchmark method is called to trial the algorithm over the same range of D and number of repeats as for the QWOA simulations. The ‘benchmark’ method generates a reproducible sequence of integers that are used as random seeds for all *param* functions in the `param` submodule. In this way, we ensure that the QWOA and QAOAz simulations are carried out over the same set of starting θ at the starting ansatz depth of $D = 1$.

A comparison of the two algorithms is shown in Section 6.2.1 where the $\langle \theta_f | \hat{Q} | \theta_f \rangle_{\text{ANZ}}$ was taken from the log file. For this brief comparison the QWOA $\langle \theta_f | \hat{Q} | \theta_f \rangle_{\text{ANZ}}$ outperforms the QAOAz for all $D > 1$.

7. Performance

The performance of QuOp_MPI was assessed on the ‘Magnus’ system at the Pawsey Supercomputing Center. This Cray XC40 Series

Supercomputer is a distributed system consisting of compute nodes each having 2× Intel Xeon E5-2690V3 ‘Haswell’ processors with 12 cores at 2.6 GHz and 64GB of RAM. Unless otherwise noted, each benchmarking trial was run for a program wall-time of one hour.

Scaling behaviour and wall-time for state evolution of $|\theta\rangle_{\text{QAOA}}$ and $|\theta\rangle_{\text{QWOA}}$ is shown in Figures 12 and 13 as a function of increasing system size N . As defined in Equations (12) and (21) each of the unitaries contains a phase-shift-unitary followed by a mixing-unitary. For $|\theta\rangle_{\text{QAOA}}$ these are implemented using the `diagonal` and `sparse` unitary classes and, for $|\theta\rangle_{\text{QWOA}}$, the `diagonal` and `circulant` unitary classes. Figure 12 demonstrate a computational advantage when using multiple MPI processes starting at approximately 12 qubits for $|\theta\rangle_{\text{QAOA}}$ and 13 qubits for $|\theta\rangle_{\text{QWOA}}$.

Across the range of simulated system sizes, QuOp_MPI demonstrates an ability to leverage an increasing degree of processing power with $|\theta\rangle_{\text{QAOA}}$ simulation achieving a speedup of approximately 7.8 relative to the performance of one MPI process in Figure 12 and 5.8 relative to the performance of one compute node in Figure 13. For $|\theta\rangle_{\text{QWOA}}$ the performance increase is more notable with a speedup of approxi-

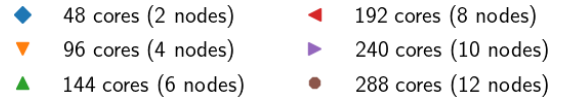
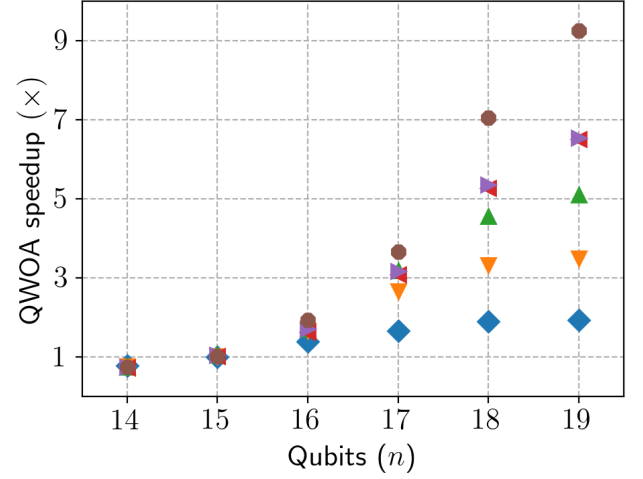
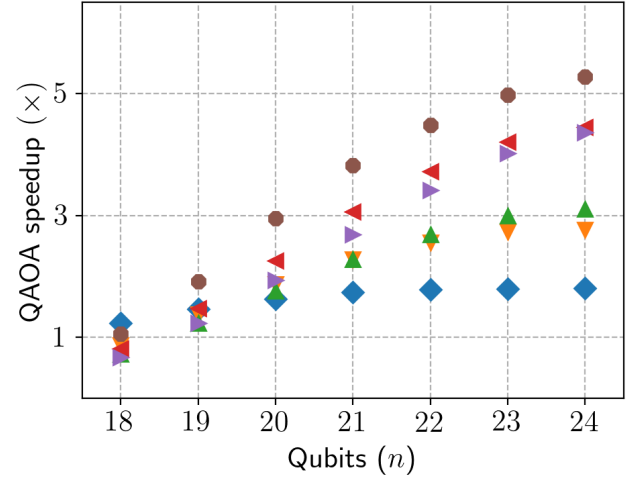
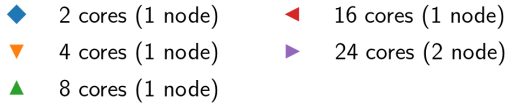
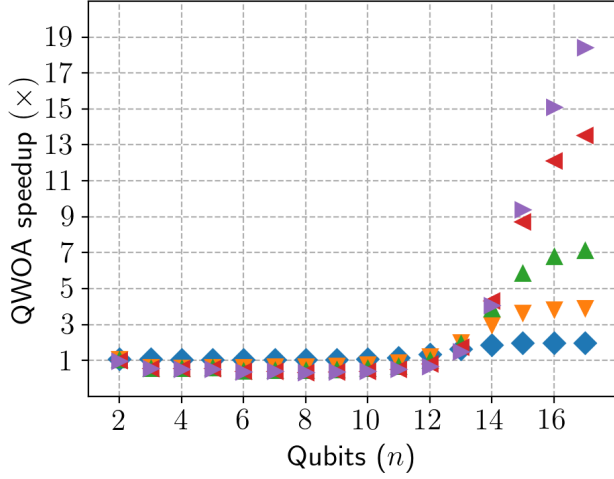
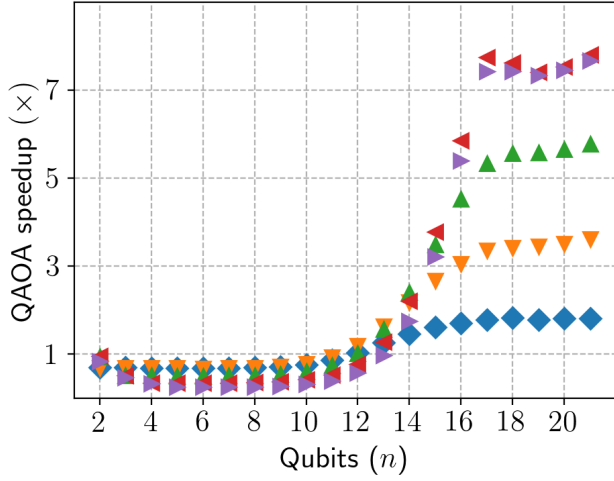


Figure 12: Speedup of the QAOA (top) and the QWOA (bottom) state evolution with an increasing number of CPU cores. For each trial, an ansatz implementing the QAOA or QWOA was prepared using the corresponding `algorithms` class with $\text{diag}(\hat{Q})$ consisting of uniformly distributed floats in $(0, 1]$. The ansatz depth was set to $D = 15$ such that calling the `Ansatz` ‘`evolve_state`’ method resulted in 15 repeats of the state evolution subroutines implementing the phase-shift and mixing-unitaries. The θ were prepared identically for all trials at the same number of qubits from the uniform distribution $(0, 2\pi]$. Speedup is reported proportional to the evolution time taken using a single CPU core (one MPI process).

mately 18.2 relative to the serial performance shown in Figure 12 and a speedup of approximately 9.1 relative to the single-node performance shown in Figure 13.

A direct comparison between single and distributed-node performance is not directly possible as the system sizes at which multiple nodes demonstrate the highest advantage exceed the simulation sizes practically achieved with a single MPI process. However, this in itself demonstrates the efficiency of massively parallel computing in QVA simulation. For both $|\theta\rangle_{\text{QAOA}}$ and $|\theta\rangle_{\text{QWOA}}$, the highest number of cores achieved the fastest simulation of the largest system over one hour of

Figure 13: Speedup of the QAOA (top) and the QWOA (bottom) state evolution with an increasing number of distributed compute nodes. For each trial, an ansatz implementing the QAOA or QWOA was prepared as described in Figure 12. Speedup is reported with respect to the evolution time taken by a single compute node with 24 CPU cores (24 MPI process).

program wall-time with $|\theta\rangle_{\text{QAOA}}$ computed for a system of 26 qubits using 14 nodes in approximately 31 minutes and $|\theta\rangle_{\text{QWOA}}$ computed for a system of 21 qubits using 15 nodes in approximately 21 minutes.

To validate the state evolution results the state norm was recorded for each of the evolved states considered in Figures 12 and 13. By default, the underlying FFTW library used for QWOA mixing-unitary evolution targets single precision accuracy and the exponentiation library used to compute the QAOA mixing-unitary evolution targets double-precision accuracy. The maximum observed deviation from the norm of -2.39×10^{-9} for the QWOA evolution and -5.05×10^{-13} for the QAOA evolution is consistent with these precision targets.

The effectiveness of the various optimisation algorithms included with the SciPy and NLOpt packages was considered with respect to the simulation of the QAOA and the QWOA. To do so we adopted the

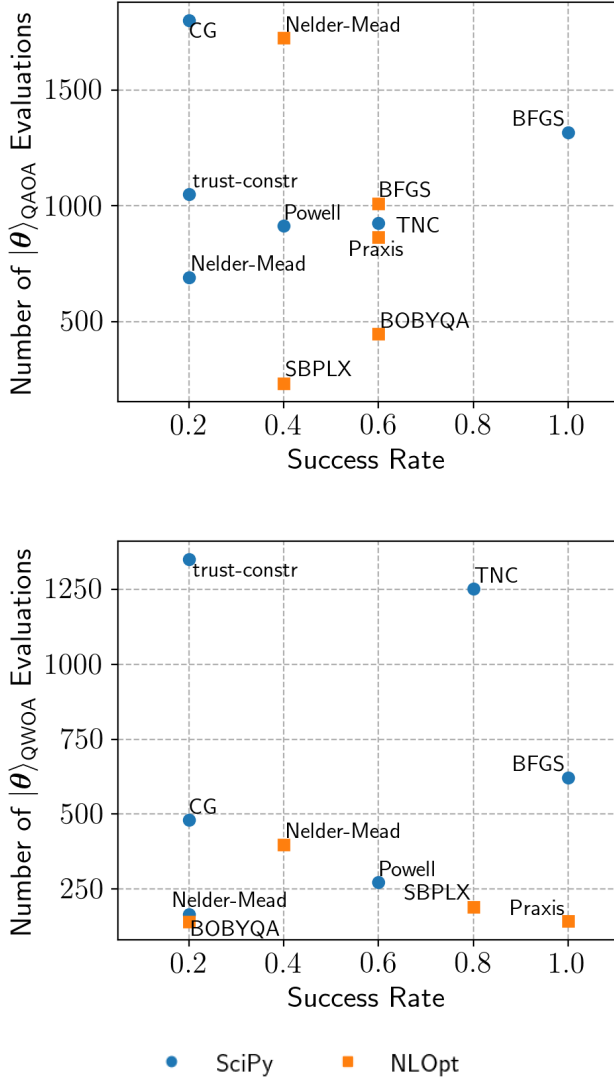


Figure 14: A comparison of the optimisation algorithms included with the SciPy and NLOpt packages. The plots depict algorithms that satisfied the convergence criteria in at least one out of the five trials. The completed list of considered algorithms is as follows. SciPy: BFGS, CG, Nelder-Mead, trust-constr, Powell. NLOpt: TNC, LD_LBFGS, LN_BOBYQA, LN_PRAXIS, LN_NELDERMEAD, LN_SBPLX, LD_MMA, LD_CCSAQ. The comparison was carried out on 17 nodes over a period of 48 hours.

method outlined in the NLOpt documentation [28]. In each instance, a system of 16 qubits ($N = 2^{16}$) was considered with a randomly generated $\text{diag}(\hat{Q})$ consisting of values from a uniform distribution over $(0, 1]$. Five sets of θ were generated for $D = 5$ ($|\theta| = 10$) and the algorithms were simulated using various optimisation algorithms provided by SciPy and NLOpt (as listed in the caption of Figure 14). For each of the five θ sets the lowest objective function value was used to define five instances of the modified objective function

$$f'(\theta) = |\min(f_{\text{ANZ}, \theta_i}) - f_{\text{ANZ}}(\theta)|, \quad (32)$$

where $\min(f_{\text{ANZ}, \theta_i})$ is the minimum objective function value found by any of the considered optimisation algorithms with initial variational parameters θ_i . Each optimisation algorithm was then trialled with starting parameters θ_i and the objective function defined as in Equation (32). A particular algorithm was considered to have ‘succeeded’

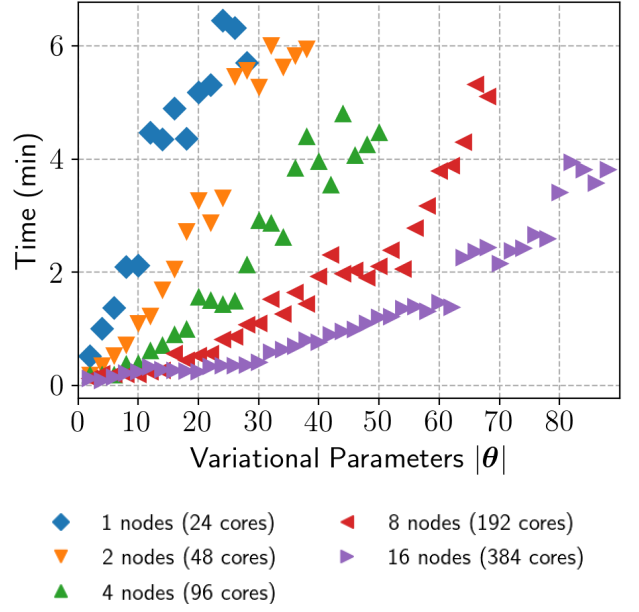


Figure 15: In-program time taken to execute QWOA as defined in Figure 12 using parallel evaluation of $\nabla_{\theta} f_{\text{ANZ}}$. For all simulations the BFGS optimisation algorithm was used with a target tolerance of 1^{-8} and $\nabla_{\theta} f_{\text{ANZ}}$ was approximated using forward differences.

if it satisfied $f'(\theta) < 0.08$.

For the QAOA trials the minimum $\langle \theta_f | \hat{Q} | \theta_f \rangle_{\text{QAOA}}$ were 0.162 (Powell), 0.156 (BFGS), 0.120 (BOBYQA), 0.228 (LD_LBFGS) and 0.154 (LD_LBFGS), and for the QWOA the $\langle \theta_f | \hat{Q} | \theta_f \rangle_{\text{QWOA}}$ were 0.074 (BFGS), 0.086 (LN_SBPLX), 0.078 (BFGS), 0.06 (BFGS) and 0.073 (Powell). As shown in Figure 14, BFGS was the only algorithm to consistently satisfy the convergence test for both the QAOA and the QWOA. This result, in combination with a relatively low number of associated $|\theta\rangle_{\text{ANZ}}$ evaluations, supports the use of BFGS as the default QuOp_MPI optimisation algorithm.

Figure 12 examines the in-program time taken to execute the QWOA with an increasing number of θ using parallel evaluation of $\nabla_{\theta} f_{\text{ANZ}}$. For Figure 15 an optimisation problem with $S' = 2^{16}$ was simulated with one to sixteen nodes with one MPI sub-communicator per node. The parallel advantage afforded by the additional layer of parallelism is evident with 16 nodes completing simulations up to $|\theta| = 88$ within a one-hour program wall-time as compared to the maximum of $|\theta| = 28$ for a single node. Notably, computation of $|\theta_f\rangle_{\text{QWOA}}$ at this scale was observed to not scale strongly past one compute node (see Figure 13 (bottom)). As such, parallel evaluation of $\nabla_{\theta} f_{\text{ANZ}}$ affords a degree of scalability that is not otherwise achievable.

The minimum objective function value achieved for each trial in Figure 15 is shown in Figure 16. Overall, the $\langle \theta_f | \hat{Q} | \theta_f \rangle_{\text{QWOA}}$ is observed to asymptotically decrease towards $\min(\hat{Q})$ as expected.

8. Conclusion

QuOp_MPI provides a highly scalable and flexible platform for parallel simulation and design of QVAs. As shown by examples, researchers are able to quickly write programs to simulate several previously studied quantum optimisation algorithms, including the QAOA, ex-QAOA, QWOA and QAOAz, capable of running efficiently on a massively parallel systems with minimal background in parallel computing.

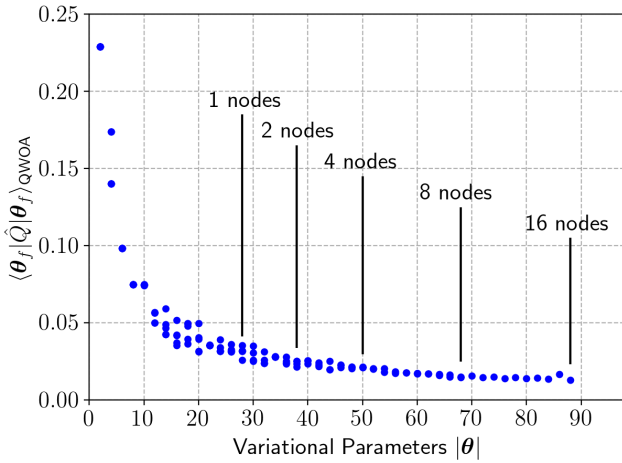


Figure 16: The optimised objective function $\langle \theta_f | \hat{Q} | \theta_f \rangle_{\text{QWOA}}$ for QWOA simulations as described in Figure 15 using 1, 2, 4, 8 and 16 compute nodes. Markers indicate the maximum number of qubits simulated using the noted number of nodes with a program wall-time of one hour.

While this introduction to the package has focused on combinatorial optimisation following a pattern of alternating phase-shift and mixing-unitaries, the flexibility afforded of QuOp.MPI allows for exploration of QVAs beyond this paradigm. Also not explored has been the application of QuOp.MPI to the simulation of quantum variational eigensolver algorithms which, while falling within the simulation framework of QuOp.MPI, lie outside the immediate research interests of the authors.

Currently, QuOp.MPI supports the efficient simulation of sparse and circulant mixing operators. While this covers the majority of mixing operators considered in the literature of QVAs, the inclusion of a unitary class supporting dense matrix-operators would significantly increase the scope of possible simulation. The inclusion of such a class is slated for a future update.

Acknowledgements

This work was supported by resources provided by the Pawsey Supercomputing Centre with funding from the Australian Government and the Government of Western Australia. EM acknowledges the support of the Australian Government Research Training Program Scholarship. The authors would like to thank Sam Marsh, Nicholas Slate, Tavis Bennett, Mark Walker, Burbukje Shakjiri, Andrew Freedland, Zecheng Li, Yuhui Wang and Jianing Sun for their valuable feedback and code testing during the development of QuOp.MPI.

References

- [1] D. Matthews, How to get started in quantum computing, *Nature* 591 (2021) 166.
- [2] M. Cerezo, A. Arrasmith, R. Babbush, et al., Variational quantum algorithms, *Nature Review Physics* 3 (2021) 625.
- [3] E. Farhi, J. Goldstone, S. Gutmann, A Quantum Approximate Optimization Algorithm, arXiv:1411.4028 [quant-ph] (2014).
- [4] S. Hadfield, Z. Wang, B. O’Gorman, E. G. Rieffel, D. Venturelli, R. Biswas, From the Quantum Approximate Optimization Algorithm to a Quantum Alternating Operator Ansatz, *Algorithms* 12 (2019) 34.
- [5] S. Marsh, J. B. Wang, Combinatorial optimization via highly efficient quantum walks, *Quantum Information Processing* 18 (2019) 61.

- [6] S. Marsh, J. B. Wang, Combinatorial optimization via highly efficient quantum walks, *Physical Review Research* 2 (2020) 023302.
- [7] G. G. Guerreschi, M. Smelyanskiy, Practical optimization for hybrid quantum-classical algorithms, arXiv:1701.01450 [quant-ph] (2017).
- [8] A. Peruzzo, J. McClean, P. Shadbolt, M.-H. Yung, X.-Q. Zhou, P. J. Love, A. Aspuru-Guzik, J. L. O’Brien, A variational eigenvalue solver on a photonic quantum processor, *Nature Communications* 5 (2014).
- [9] J. Preskill, Quantum Computing in the NISQ era and beyond, *Quantum* 2 (2018) 79.
- [10] D. B. Kell, Scientific discovery as a combinatorial optimisation problem: How best to navigate the landscape of possible experiments?, *Bioessays* 34 (2012) 236.
- [11] F. F. S. Sánchez, C. A. L. Lazo, F. Y. S. Quiñónez, Comparative Study of Algorithms Metaheuristics Based Applied to the Solution of the Capacitated Vehicle Routing Problem, IntechOpen, 2020.
- [12] R. Liu, X. Li, K. S. Lam, Combinatorial Chemistry in Drug Discovery, Current opinion in chemical biology 38 (2017) 117–126.
- [13] R. C. Lozano, M. Carlsson, G. H. Blindell, C. Schulte, Combinatorial Register Allocation and Instruction Scheduling, *ACM Transactions on Programming Languages and Systems* 41 (2019) 17:1–17:53.
- [14] H. Markowitz, Portfolio Selection, *J. Finance* 7 (1) (1952) 77–91.
- [15] A. Palczewski, LP Algorithms for Portfolio Optimization: The PortfolioOptim Package, *R J.* 10 (2018) 308–327.
- [16] D. Willsch, M. Willsch, F. Jin, K. Michielsen, H. De Raedt, GPU-accelerated simulations of quantum annealing and the quantum approximate optimization algorithm, arXiv:2104.03293 [physics, physics:quant-ph] (2021).
- [17] E. Matwiejew, QuOp.MPI (v1.0.0). URL <https://github.com/Edric-Matwiejew/QuOp.MPI/releases/tag/v1.0.0>
- [18] M. Broughton, G. Verdon, T. McCourt, A. J. Martinez, J. H. Yoo, S. V. Isakov, P. Massey, M. Y. Niu, R. Halavati, E. Peters, M. Leib, A. Skolik, M. Streif, D. Von Dollen, J. R. McClean, S. Boixo, D. Bacon, A. K. Ho, H. Neven, M. Mohseni, TensorFlow Quantum: A Software Framework for Quantum Machine Learning, arXiv:2003.02989 [cond-mat, physics:quant-ph] (2020).
- [19] A. J. McCaskey, D. I. Lyakh, E. F. Dumitrescu, S. S. Powers, T. S. Humble, XACC: a system-level software infrastructure for heterogeneous quantum-classical computing, *Quantum Science and Technology* 5 (2020) 024002.
- [20] B. Villalonga, S. Boixo, B. Nelson, C. Henze, E. Rieffel, R. Biswas, S. Mandrà, A flexible high-performance simulator for verifying and benchmarking quantum circuits implemented on real hardware, *npj Quantum Information* 5 (2019) 1–16.
- [21] P. Crescenzi, V. Kann, R. Silvestri, I. L. Trevisan, Structure in Approximation Classes, *SIAM Journal on Computing* 28 (1999) 24.
- [22] M. Frigo, S. G. Johnson, The Fastest Fourier Transform in the West: (1997).
- [23] M. Frigo, S. Johnson, The Design and Implementation of FFTW3, *Proceedings of the IEEE* 93 (2005) 216–231.
- [24] E. Matwiejew, J. B. Wang, QSW.mpi: A framework for parallel simulation of quantum stochastic walks, *Computer Physics Communications* 260 (2021) 107724.
- [25] L. Zhou, S.-T. Wang, S. Choi, H. Pichler, M. D. Lukin, Quantum Approximate Optimization Algorithm: Performance, Mechanism, and Implementation on Near-Term Devices, *Physical Review X* 10 (2020) 021067.
- [26] J. Nocedal, S. J. Wright, Numerical optimization, 2nd Edition, Springer series in operations research, Springer, New York, 2006.
- [27] E. Jones, T. Oliphant, P. Peterson, SciPy: Open source scientific tools for Python (2001). URL <http://www.scipy.org/>
- [28] S. G. Johnson, The NLOpt nonlinear-optimization package. URL <http://github.com/stevengj/nlopt>
- [29] D. Steinberg, revrand. URL <https://travis-ci.org/github/NICTA/revrand>
- [30] N. Slate, E. Matwiejew, S. Marsh, J. B. Wang, Quantum walk-based portfolio optimisation, *Quantum* 5 (2021) 513.
- [31] pandas-datareader, version Number: 0.10.0. URL <https://github.com/pydata/pandas-datareader/>
- [32] Yahoo Finance – stock market live, quotes, business & finance news. URL <https://au.finance.yahoo.com/>



Edric Matwiejew is a PhD candidate at the University of Western Australia with the Quantum Information, Algorithms and Simulation research centre led by Professor Jingbo Wang. He develops software for the high-performance simulation of quantum systems, which he applies to the design of quantum algorithms with near-term applications. In his downtime, he enjoys re-imagining scientific concepts in modular synthesizer design.



Professor Jingbo Wang is the Director of QUIZA Research Centre (<https://quiza.tech/>) hosted at The University of Western Australia, leading an active group in the area of quantum information, simulation, and algorithm development. Prof Wang and her team pioneered quantum walk-based algorithms to solve problems of practical importance otherwise intractable, which include complex net-

work analysis, graph theoretical studies, machine learning, and combinatorial optimization. She is currently also the Head of Physics Department, Deputy Head of School of Physics, Mathematics and Computing, and Chair of QST (Quantum Science and Technology) Topical Group under the Australian Institute of Physics.